Proceedings of the Combustion Institute 40 (2024) 105763

Contents lists available at ScienceDirect

Proceedings of the Combustion Institute

journal homepage: www.elsevier.com/locate/proci

An experimental marker of thermo-diffusive instability in hydrogen-enriched flames

Oussama Chaib [a,*], Simone Hochgreb [a], Isaac Boxx [b,c]

[a] Department of Engineering, Cambridge University, Cambridge CB2 1PZ, United Kingdom
[b] Institute of Combustion Technology, German Aerospace Center (DLR), Stuttgart 70569, Germany
[c] Chair of Optical Diagnostics for Energy, Process and Chemical Engineering, RWTH Aachen University, Aachen 52062, Germany

ARTICLE INFO

Keywords:
Hydrogen flames
Thermo-diffusive instability
Flame speed
Curvature

ABSTRACT

The structure of hydrogen-enriched methane-air flames in a Bunsen burner at low turbulence is investigated using OH planar laser-induced fluorescence (PLIF). Three flames are investigated at identical unstretched laminar flame speeds and turbulence conditions, while hydrogen enrichment is varied up to 70% by volume. An increase in global flame consumption speed is recorded with hydrogen addition, and is attributed to both an increase in flame surface area and fluctuations in stoichiometry along the flame surface as a result of differential diffusion. These fluctuations are found to be well-captured by the gradient of OH-PLIF intensity along the flame front and it is hence identified as a promising experimentally-accessible marker of thermo-diffusive instability. Its correlation with curvature is hereby examined for the first time experimentally. No correlations are found in absence of hydrogen, while increasingly positive correlations are recorded with hydrogen enrichment, consistent with the behavior of local fuel consumption in direct numerical simulations (DNS) of lean hydrogen-air flames. This highlights the potential of OH intensity gradient magnitudes as a marker of thermo-diffusive instability, and a potential surrogate for local fuel consumption speed which is inaccessible experimentally.

1. Introduction

Amidst the current pressing environmental issues and growing sustainability concerns, the need for flexible and versatile low-carbon combustion technologies has never been more imperative. The resurgence of hydrogen in the energy landscape reignites discussions on its integration in modern-day premixed lean-burn technologies, potentially through controlled blends of hydrogen and conventional hydrocarbon fuels (i.e., natural gas), which can play a pivotal role in reducing carbon emissions while allowing for stable operation over a wider range of lean conditions [1–3]. Lean premixed hydrogen-air flames are however prone to thermo-diffusive (TD) instabilities which arise from differential diffusion effects (imbalance between thermal and mass diffusivities), yielding sub-unity effective Lewis numbers [4]. This favors the formation of bulge-like cellular structures where the local burning rate along the flame surface is heavily influenced by the sign of curvature [5–8]. Local flame speeds can thereby exceed their corresponding laminar values by a factor of 2 to 5 at similar turbulence and operating conditions [9]. This enhancement is known to be driven by two key mechanisms: (1) the increase in flame surface area, (2) a local enhancement in fuel consumption rate per unit area in bulges convex to the unburnt reactants, as a result of the instability [10]. The latter is typically described by a non-dimensional quantity I_0, referred to as the stretch factor.

To better understand these behaviors, a substantial body of DNS work examined the correlation between flame consumption speed and curvature in lean hydrogen-air flames [5,6,11–15]. We highlight, for example, the early 2D flame-in-a-box simulations of Baum et al. [11] which revealed the existence of strong positive correlations between heat release rate, flame consumption speed, and curvature in such flames. Direct, spatially resolved measurements of heat release or fuel consumption are hardly feasible experimentally, which compelled the authors to express their findings in terms of experimentally-measurable quantities. The OH radical, accessible via planar laser-induced fluorescence, emerged as the primary candidate. OH-PLIF signal intensity I_{OH} is indeed proportional to the local concentration, and thus molar fraction of the OH radical, X_{OH}. Correlations between X_{OH} and curvature were hence examined in a series of DNS papers by Bell et al. [5] and Day et al. [13,16]. They uncovered strong positive correlations between the local flame speed and peak OH molar fractions along the flame normal in DNS of lean hydrogen-air flames. The authors

* Corresponding author.
E-mail address: oc327@cam.ac.uk (O. Chaib).

https://doi.org/10.1016/j.proci.2024.105763
Received 3 December 2023; Accepted 7 August 2024
Available online 4 September 2024
1540-7489/© 2024 The Authors. Published by Elsevier Inc. on behalf of The Combustion Institute. This is an open access article under the CC BY license (http://creativecommons.org/licenses/by/4.0/).

Table 1
Experimental conditions investigated in this study. The bulk flow velocity U_0 was estimated based on the total mass flow rate of reactants $\dot{m}$. The root-mean-square axial velocity u' was measured via particle-image velocimetry (PIV) [17]. The integral lengthscale was obtained from scaling estimates $l_t \approx (u'/U_0)d$. The Karlovitz number is hereby defined as $\mathrm{Ka} = (u'/s_L^0)^{3/2}(l_t/\delta_L^0)^{-1/2}$. The effective Lewis number $\mathrm{Le_{eff}}$ is estimated as $\mathrm{Le_{eff}} = 1 + \left[(\mathrm{Le_{ox}} - 1) + (\mathrm{Le_f} - 1)A\right]/(1 + A)$, where subscripts $_{ox}$ and $_f$ refer to oxidizer and fuel, respectively, and $A = 1 + \mathrm{Ze}(1/\phi - 1)$ is a mixture strength parameter [4]. The bi-fuel mixture effective Lewis number is estimated using the volumetric weighted approach: $\mathrm{Le_f} = \chi \mathrm{Le_{H_2}} + (1 - \chi)\mathrm{Le_{CH_4}}$, while the Zel'dovich number is obtained using Law and Sung's method [4,18]. All thermodynamic quantities were obtained from 1D simulations of freely-propagating unstretched laminar flames using the GRI-Mech 3.0 mechanism [19,20].

Case	χ [%]	ϕ [–]	s_L^0 [m s^{-1}]	δ_L^0 [mm]	U_0 [m s^{-1}]	u' [m s^{-1}]	l_t [mm]	Ka [–]	$\mathrm{Le_{eff}}$ [–]
1	0	1.00	0.38	0.44	2.13	0.26	3.20	0.21	1.04
2	40	0.80	0.38	0.44	2.18	0.28	3.30	0.23	0.88
3	70	0.65	0.35	0.47	2.12	0.26	3.20	0.25	0.70

highlight this as a potential avenue to infer local fuel consumption rates from the experimentally-measured OH-PLIF intensities [5,16]. In a follow-up study, Day et al. [13] identify the OH intensity gradient magnitude $G = |\nabla I_{OH}|$ at the flame front as a key indicator of burning intensity from PLIF images. This information is, however, only used to improve the flame detection routine, with no attempt to examine quantitative correlations with curvature experimentally, despite the striking correlations in the supporting PLIF images. It is also worth noting these computational studies focused on single-fuel mixtures only (either pure methane, or pure hydrogen), due to the kinetic complexity of H_2/CH_4 blends and the high computational cost it entailed for DNS at the time. Hence, there is a need to re-visit these correlations in the context of hydrogen/methane-air flames of variable blending ratios both computationally and experimentally.

In this work, we examine the effect of hydrogen enrichment (up to 70% by volume) on the structure of turbulent, premixed methane-air flames via OH-PLIF. Global flame speed measurements are provided, and the contribution of both flame wrinkling and the stretch factor is evaluated at varying hydrogen blending ratios. The OH intensity gradient magnitude G along the flame surface is identified as a promising indicator of thermo-diffusive instability in hydrogen-enriched flames. For the first time, quantitative correlation statistics of G vs. curvature are examined. These demonstrate an increasingly positive correlation with hydrogen addition, consistent with DNS findings. The results of this study provide valuable insights into the potential surrogate role of G in capturing the correlation originally established between local flame consumption speed and curvature in the literature.

2. Experimental methodology

2.1. Configuration and diagnostics

Measurements were conducted in flames generated with the DLR Bunsen Burner, described extensively in previous work [17,21]. It consists of a cylindrical plenum that terminates at a high blockage ratio ($\approx 96\%$) turbulence generator plate composed of four axisymmetric circular holes of diameter 4.8 mm. After the plenum, flow passes through a conical nozzle (contraction angle 15 degrees), to a short (1 cm long) straight section of 15 mm diameter, before exiting to atmospheric pressure.

Three test cases were measured in this study, as listed in Table 1. Case 1 was a methane-air flame. Cases 2 and 3 were methane/hydrogen-air flames. The burner was operated at low velocity and turbulence characteristics were kept constant in all the conditions investigated. The unstretched laminar flame speed was kept constant by tuning down equivalence ratios ϕ as hydrogen was added to the reactant flow. All three flames are in the wrinkled flamelet regime.

Flames were imaged using a high-speed (10 kHz) OH-PLIF imaging system, described extensively in the cited papers [21,22]. The setup consisted of a frequency-doubled dye laser, pumped by a high-speed, pulsed Nd:YAG laser (Edgewave IS400-2-L, 150 W at 532 nm and 10 kHz) and an intensified (LaVision HS-IRO) high-speed CMOS camera system (LaVision HSS6). The dye laser system (Sirah Credo) produces approximately 5.3 to 5.5 W at 283 nm and 10 kHz repetition rate (i.e. 0.53–0.55 mJ/pulse) and was tuned to excite the $Q_1(6)$ line of the $A^2\Sigma^+ - X^2\Pi$ ($v' = 1$, $v'' = 0$) band. The laser beam is formed into a 50 mm (high) × 0.2 mm (thick) sheet using three fused-silica, AR-coated cylindrical lenses. The OH-PLIF camera was equipped with a UV-capable objective lens (Cerco, f = 100 mm, f/2.8) and a bandpass filter (300–325 nm). The projected pixel resolution was 0.0704 mm/px, with an array size of 768 × 768 px^2. A total of 19400 12-bit grayscale images were collected for each experimental condition.

2.2. Data processing

The image processing methodology used in this study was described extensively in our previous work [21]. A combination of nonlinear edge-preserving filters (bilateral and anisotropic diffusion) is used for denoising. The instantaneous position of the flame front is then determined using the *hybrid filtered Canny* algorithm [21] which combines segmentation and edge detection. The final flame front outlined by the algorithm corresponds to the instantaneous location of peak OH intensity gradient magnitudes in the image, which is a common tracer of the flame front [21]. The flame surface density Σ is defined as the ensemble-average perimeter of the flame fronts within 1×1 px^2 interrogation windows divided by the area of the window [23]. The single-shot flame fronts are also used to binarize the image into products and reactants and a mean progress variable $\bar{c}$ is hence defined as the ensemble-average of binarized OH-PLIF images [23].

Two-dimensional OH gradient magnitudes G are computed from the filtered PLIF images using a derivative of Gaussian (DoG) kernel of standard deviation 2, and are normalized by maxima to account for shot-to-shot variations in laser pulse energies. We note the choice of kernel had negligible effects on the obtained values of (normalized) gradients in this work and similar results were achieved using alternative kernels such as the Sobel operator. The relevant scalar quantities (OH intensity gradient magnitudes G and two-dimensional curvatures κ) are extracted along the curvilinear coordinate of the flame front defined by the arc length s. The two-dimensional curvature is obtained using the equation:

$$\kappa = \frac{x'z'' - x''z'}{(x'^2 + z'^2)^{3/2}} \tag{1}$$

where $x' = \frac{dx}{ds}$ and $z' = \frac{dz}{ds}$. Derivatives with respect to the curvilinear coordinate are estimated by fitting a second-order polynomial using the nearest 20 adjacent points (10 on either side) [7,24]. Points are assigned positive curvature values if their center of curvature is located in the burnt side and negative curvature values if it is located in the unburnt side.

2.3. Flame speed definition

The global consumption speed of a statistically-steady turbulent envelope flame is defined as [25]:

$$s_T = \frac{\dot{m}}{\rho_u A_0} \tag{2}$$

where $\dot{m}$ and ρ_u refer to the mass flow rate and density of the unburnt mixture, respectively. The reference area A_0 is chosen as the surface area of the mean progress variable $\bar{c} = 0.5$ [23,25].

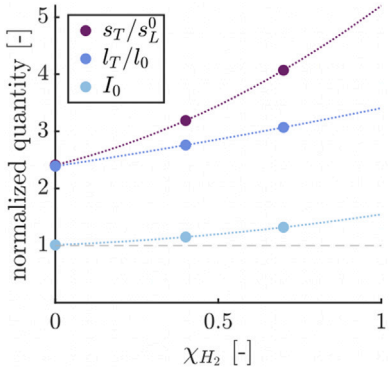

Fig. 1. Measured consumption speed enhancement s_T/s_L^0, flame wrinkling term l_T/l_L, and resulting stretch factors I_0 obtained for each condition. Dotted lines are best polynomial fits (for visibility only). The gray dashed line refers to the unity I_0 threshold.

In 2D, the enhancement in flame consumption speed (relative to a laminar unstretched flame) can be written as the product of a flame wrinkling term l_T/l_0 and a stretch factor I_0 [6]:

$$\frac{s_T}{s_L^0} = \frac{l_T}{l_0} I_0 \tag{3}$$

This allows a distinction between the two mechanisms responsible for the enhancement in consumption speed and is especially pertinent to the analysis of TD-unstable flames where the stretch factor I_0 is used to quantify the contribution of the varying local reactivity along the flame, induced by the instability [6,15]. In this work, the turbulent flame length l_T is measured as the integral of the flame surface density in the 2D imaging plane, while the reference iso-length l_0 corresponds to the perimeter of the mean flame surface ($\bar{c} = 0.5$). Consumption speeds reported in this work are hence estimated using Eq. (2) and corresponding stretch factors are obtained by solving Eq. (3) for I_0.

3. Flame speed measurements

Normalized global consumption flame speed measurement values for each experimental condition are shown in Fig. 1 with details provided in Table 2. The flame consumption speed increases with hydrogen enrichment with the largest increase (≈ 69%) recorded in Case 3. Flame wrinkling is the only contributor to flame speed enhancement in the pure methane-air flame (Case 1). The corresponding stretch factor takes a value of unity, which is consistent with past studies of TD-stable flames [6,9,25]. In this case, the local flame propagation is comparable to that of a laminar unstretched flame and the increase in flame consumption speed is attributed to the effect of turbulence which increases the total flame surface area. The flame wrinkling term l_T/l_L and the stretch factor I_0 increase in tandem as hydrogen is added to the unburnt mixture. Flame wrinkling remains the major driver of the enhancement in flame speed in the hydrogen-containing flames, but the overall area enhancement is insufficient to account for the overall consumption rate. Area increase accounts for 75% of the increase in s_T/s_L^0 in Case 3. The remaining effect is attributed to enhanced burning owing to TD instability effects. It is worth noting that the observed increase in flame surface area itself may be partly attributed to differential diffusion effects, given turbulence conditions are kept constant in all three cases. This suggests an intricate connection between both flame speed enhancement mechanisms in TD-unstable flames and a visual interpretation is presented in the next section.

Table 2
Measured terms of Eq. (3) for each experimental condition. Values are rounded to the nearest two decimal places.

Case	s_T/s_L^0	l_T/l_0	I_0
1	2.41	2.39	1.01
2	3.19	2.76	1.15
3	4.07	3.07	1.32

4. Flame morphology

4.1. Cellular structures

Representative PLIF images from each experimental condition are shown in Fig. 2. The flame surfaces display the typical features of turbulent flames, namely a wrinkled front populated by a number of concave and convex surfaces. For the sake of clarity, we shall refer to these structures as *crests* ($\kappa < 0$) and *troughs* ($\kappa > 0$), respectively. With increasing hydrogen enrichment, the wrinkledness of the front is more pronounced, which gives rise to a number of small cellular structures. This results in an enhancement of flame surface area and is consistent with the increase in the flame wrinkling term l_T/l_L observed in Fig. 1.

The evolution in flame front morphology is accompanied by a notable shift in the signal magnitude of LIF of OH radicals in the products, wherein the intensity peak migrates to the trailing edge of troughs. A similar observation can be made from the OH-PLIF signal intensity gradient profiles along the flame front. These profiles are relatively homogeneous in Case 1, with no discernible preference to the sign of curvature. They become less homogeneous with hydrogen addition and a preference towards troughs is observed, leading to increased OH-PLIF signal gradients in their vicinity. This trend is indicative of local fluctuations in stoichiometry as a result of differential diffusion and is consistent with the increase in the stretch factor I_0 observed in Fig. 1. The focusing of hydrogen towards troughs causes these structures to burn more intensely, thereby increasing the super-equilibrium concentration of the OH radical (brighter OH intensities) at their trail. Conversely, the reactant mixture in the vicinity of crests is leaner which causes them to burn less intensely with significantly lower super-equilibrium OH concentrations (dimmer OH intensities) at their trail.

These observations strengthen the argument for a synergistic interaction between both flame speed enhancement mechanisms in TD-unstable flames, as observed in direct numerical simulations of Berger et al. [10]. The more pronounced curvature of the flame front favors the focussing (defocussing) of hydrogen in troughs (crests) which results in significant fluctuations of equivalence ratio, and hence rate of burning, along the flame surface.

4.2. Flame fingers

Flame fingers have also been observed in the hydrogen-rich case as illustrated in the contour plots in Fig. 3a. These are typically thin elongated crests protruding into the products region. The two flame fingers shown in Fig. 3 are flanked by convex troughs of intense burning, as evidenced by the high super-equilibrium OH regions ($I_{OH} = 0.8 - 0.9$) at their trail. The OH profile in the vicinity of these fingers appears significantly thicker which suggests a lower burning intensity locally. Gradients of OH intensities decrease considerably ($G < 0.3$) as they approach their tip (Fig. 3b) which yields breaks or discontinuities in the flame front (traced in black dots), possibly due to local extinctions, as was found in previous direct numerical simulations [5,12,13]. The sign of curvature appears to dictate the behavior of G in Fig. 3b where a clear contrast between crests and troughs is observed. This echoes the trends observed in Fig. 2, indicating a positive correlation with curvature in the TD-unstable hydrogen-rich case. In fact, the OH-PLIF intensity gradient profile portrayed in Fig. 3b bears a striking resemblance to profiles of fuel consumption rates in DNS of lean hydrogen-air flames (see for example Figure 3c in [5] and Figure 3a in [12]). The behavior of G captures, at least qualitatively, the expected variation in local consumption speed along a flame surface subject to thermo-diffusive effects.

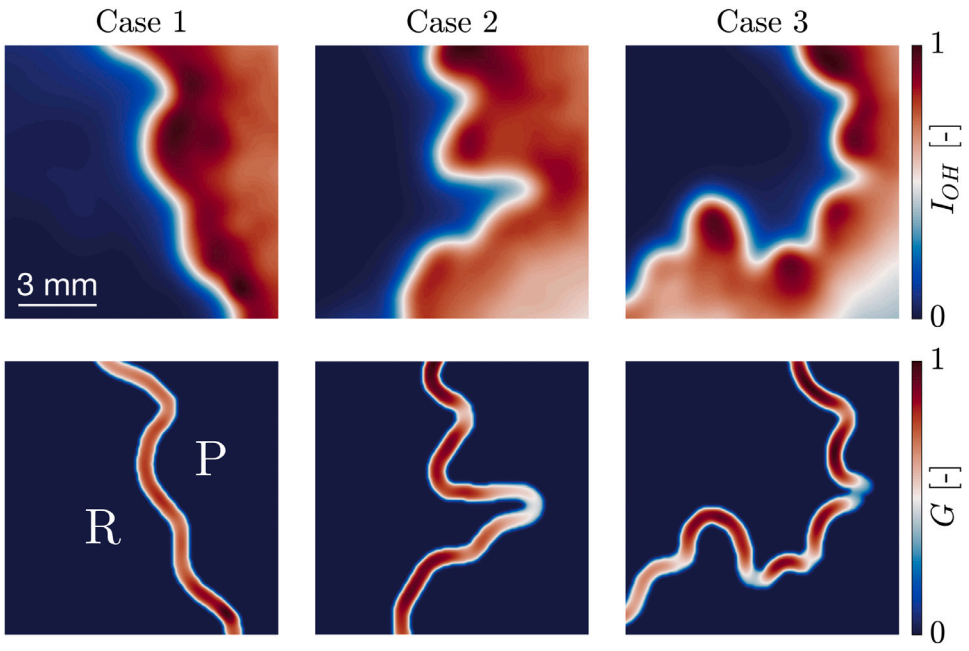

Fig. 2. Close-up view of representative flames for each experimental condition. Filtered PLIF images (normalized by maxima) and their respective gradients are illustrated in the first and second row respectively. Only gradients in the vicinity of the flame front are shown for visibility purposes. Symbols 'R' and 'P' refer to reactants and products respectively.

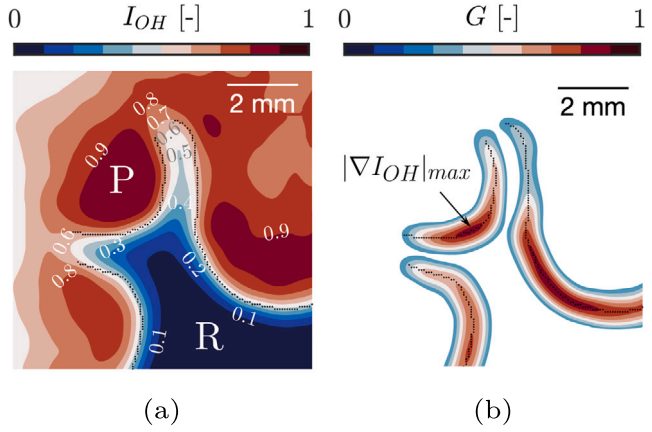

Fig. 3. (a) Contour plot of OH-PLIF intensities I_{OH} near two flame fingers from Case 3. Black dots correspond the location of the flame front marked by $|\nabla I_{OH}|_{max}$. Symbols 'R' and 'P' refer to reactants and products respectively. (b) Contour plot of corresponding OH intensity gradients G.

These results suggest OH intensity gradient magnitudes can serve as a surrogate marker of TD instability, as hinted at by Day et al. [13]. Motivated by the observations in Figs. 2 and 3, we formulate the hypothesis that G can effectively stand in for the local consumption speed s_c in assessing its correlation with curvature. Correlations between G and κ are both easily-accessible experimentally and could hence be used to assess TD instability of hydrogen flames. This also offers an intuitive and physically-interpretable complement to integral measurements of I_0, which provide limited information on the local burning rate along the flame. The potential of G as a marker of TD instability is hence explored in the remainder of this study.

5. OH intensity gradients as a marker of TD instability

5.1. Quantitative correlations

The observations made in Section 4 and DNS simulations suggest there should be a positive correlation between the local OH intensity gradient magnitude G and curvature κ in lean hydrogen-enriched flames. The correlation between G and κ along the arc-length of the instantaneous flame front s can be measured using the Pearson correlation coefficient R:

$$R_{G^+,\kappa^+} = \frac{\mathbb{E}(G^+\kappa^+)}{\sigma_{G^+}\sigma_{\kappa^+}} \tag{4}$$

where the plus superscript sign '+' refers to mean-centered quantities, and σ is their respective standard deviation. The mean ($\mathbb{E}$) is over all points along the arc-length of the instantaneous flame front. This yields values of R_{G^+,κ^+} in the range $[-1, 1]$, where $R = 0$ implies no correlation, while $R = 1$ ($R = -1$) implies both signals are perfectly correlated (decorrelated). An example is shown in Fig. 4 for a PLIF image from Case 3. Notice the remarkable correlation between the two quantities, both in trend and frequency. The cellular nature of the hydrogen-rich flame is well-captured by the gradient along the front and both G^+ and κ^+ appear to follow the same trends despite some differences in order of magnitude. This results in a moderate positive correlation between both quantities ($R_{G^+,\kappa^+} \approx 0.62$). Correlation statistics obtained for each condition were compiled in probability density function (pdf) histograms and are provided in Fig. 5, with further details in Table 3. These were constructed from a sample size of 17,800 to 19,000 instantaneous flame fronts per condition. The correlation pdf obtained for the methane-air flame (Case 1) is symmetric and centered around zero, implying no net correlation between G and κ. This is consistent with DNS [5] and the unity stretch factor obtained previously. It implies the local consumption speed is insensitive to the orientation of the flame surface, as expected of a TD-stable flame. The mass of the pdf is gradually shifted to the right with hydrogen enrichment which indicates an increasingly positive correlation. This mirrors the increasing trend in I_0 observed in Fig. 1 and is consistent with a more pronounced TD instability. In Case 3, the mode $R_{G^+,\kappa^+} = 0.5$ reveals a net positive but moderate correlation between G and κ. The trend towards left-skewness with hydrogen addition is more challenging to interpret. In Case 3, G and κ are seldom uncorrelated and the mass of the pdf is concentrated on the right side of the mean $R_{G^+,\kappa^+} > 0.45$. There is a possible connection here with the instability-induced enhancement in flame wrinkling l_T/l_L and its interplay with the stretch factor I_0 discussed at the end of Section 3. The cellularity of the flame

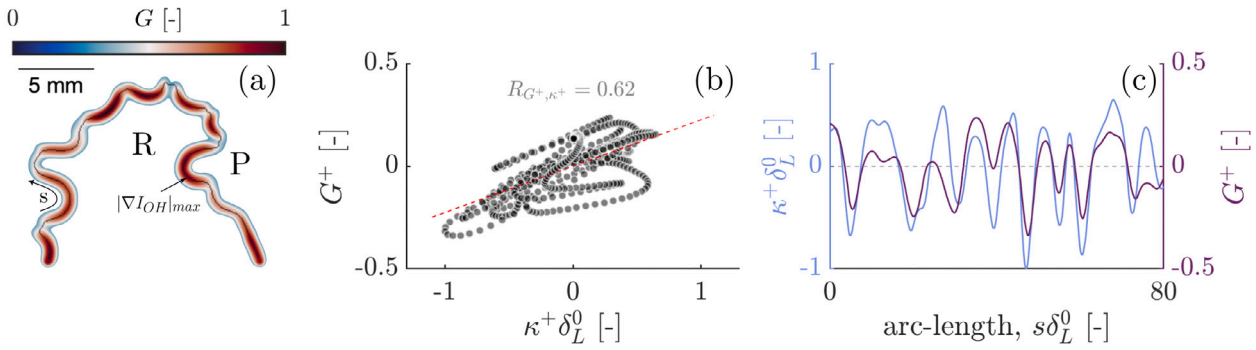

Fig. 4. (a) OH intensity gradient map for a flame front from the hydrogen-rich condition (Case 3). The flame front ($|\nabla I_{OH}|_{max}$) is marked in black color dots. The curvilinear coordinate given by the arc-length of the flame front, s, is obtained by indexing the flame front clockwise and the direction of indexing is indicated using the curved black arrow. Symbols 'R' and 'P' refer to reactants and products, respectively. (b) Scatter plot of mean-centered OH intensity gradient magnitudes G^+ and non-dimensional curvature $\kappa^+\delta_L^0$ along the flame front. The corresponding Pearson coefficient for this snapshot is written in gray color and the red dashed line shows the best linear fit. (c) Profiles of G^+ and $\kappa^+\delta_L^0$ along the flame front. (For interpretation of the references to color in this figure legend, the reader is referred to the web version of this article.)

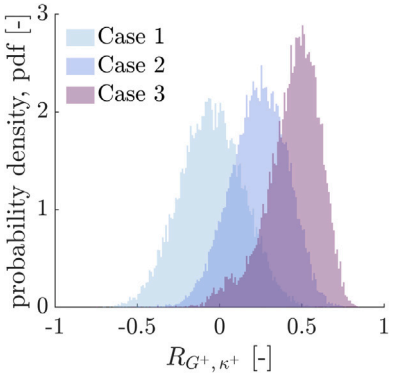

Fig. 5. Correlation probability density functions R_{G^+,κ^+} obtained for each experimental case. Bars correspond to bins of width $\Delta R_{G^+,\kappa^+} = 0.01$.

Table 3
Cross-correlation pdf properties for each experimental condition. Symbols μ, m, σ, γ_1, γ_2 refer to the mean, mode, standard deviation, skewness, and *excess* kurtosis of the cross-correlation pdf.

Case	μ	m	σ	γ_1	γ_2
1	−0.05	−0.07	0.19	0.00	−0.15
2	0.24	0.25	0.17	−0.23	−0.04
3	0.45	0.50	0.16	−0.84	1.16

front promoted by differential diffusion reduces the likelihood of flat flame surfaces, thereby enhancing curvature fluctuations and hence local fuel consumption rates along the flame surface. A parallel can be drawn with the study of Berger et al. [15] which unveiled a synergistic interaction between flame wrinkling and propensity to TD instability.

5.2. Joint probability density function histograms

Contour plots of the joint probability density function (JPDF) of G^+ and κ^+ for each condition are shown in Fig. 6. The methane-air flame (Case 1) produces a relatively symmetric and isotropic JPDF centered at zero, consistent with the zero correlation recorded for this particular case. The mass of the JPDF is evenly distributed between all four quadrants which is a further testament. With hydrogen addition, the JPDF becomes broader due to larger fluctuations in curvature and local fuel consumption along the flame. It approaches a linear shape of positive slope in Case 3 which reflects the moderate positive correlation observed previously. The mass of the JPDF migrates to the top-right quadrant $P(G^+ > 0, \kappa^+\delta_L^0 > 0) = 0.40$ in Case 3 which indicates that the bulk of the burning happens in the positively-curved flame troughs which dominate the flame surface. The tail of the JPDF in the lower-left quadrant ($G^+ < 0$, $\kappa^+\delta_L^0 < 0$) exhibits a prominent skewness in both hydrogen-containing flames which is absent in the methane-air flame. This is due to the flame fingers which burn much weakly (low gradients), occasionally feature local extinctions, and exhibit larger absolute curvatures than troughs, despite being less frequent. It is worth noting, however, that correlations in the lower-left quadrant are more prominent than those in the upper-right one. This implies that burning intensity is more sensitive to curvature in crests rather than troughs. In fact, the skewed ovoid shape and the longer tail in the lower-left quadrant in Case 3 are curiously reminiscent of the JPDF of local consumption speed and mean curvature in Day et al.'s [16] simulations of lean hydrogen-air low-swirl flames.

These results provide compelling evidence supporting the hypothesis that OH intensity gradient magnitudes can act as a surrogate for local flame consumption speeds in assessing the strength of thermo-diffusive instabilities in hydrogen-enriched flames. The observed correlations between G and κ are consistent with an evolution towards an instability-dominated regime with increasing hydrogen enrichment and aligns with the trend observed via stretch factor measurements. They complement the latter by providing a more holistic view of the dynamics of a flame surface subject to differential diffusion.

6. Conclusion

In this work, the effect of hydrogen addition to premixed methane-air flames at low turbulence and constant laminar flame speed was examined via OH-PLIF to shed light on the role of thermo-diffusive instability. An enhancement in flame speed is recorded, and is driven by both an increase in flame surface area and fluctuations in local equivalence ratios along the flame sheet. The viability of OH intensity gradient magnitudes as a marker of thermo-diffusive instability is examined via correlation statistics with curvature along the arc-length of instantaneous flame fronts. An increasingly positive correlation is recorded with hydrogen addition, while no correlation is observed in the stoichiometric methane-air flame, consistent with DNS. OH-PLIF intensity gradients capture, both qualitatively and quantitatively, the expected variation in local fuel consumption along a TD-unstable flame front and offer a more intuitive and physically-interpretable complement to global stretch factor measurements, which lack explicit information on the local burning along the flame.

Novelty and significance statement

Quantitative experimental correlations between the OH-PLIF gradient and curvature are documented for the first time in premixed flames of methane/hydrogen blends, and suggest they can be used

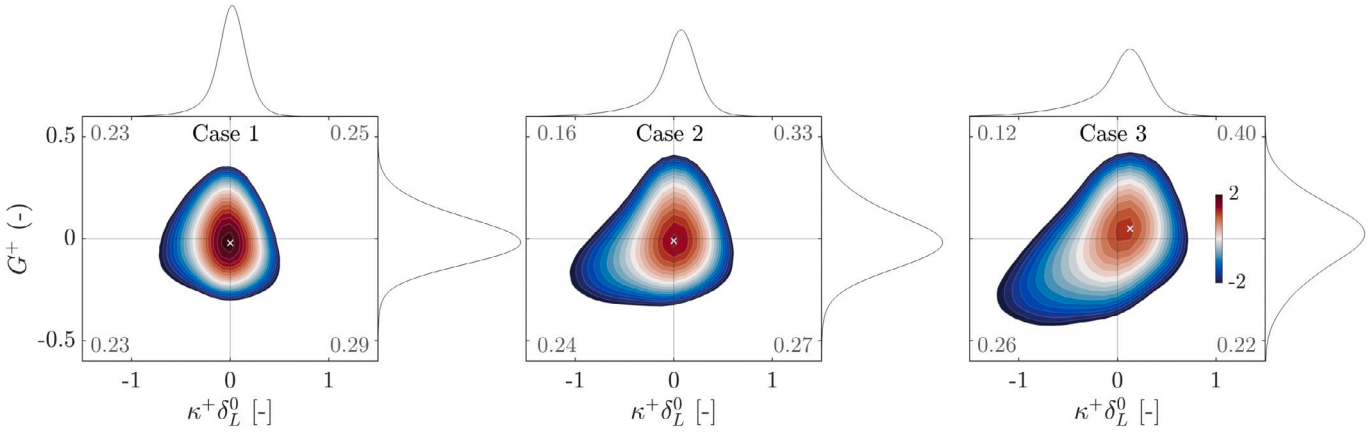

Fig. 6. Contour plots of joint probability density functions of mean-centered non-dimensional curvatures $\kappa^+\delta_L^0$ and OH intensity gradient magnitudes G^+ for each experimental condition. Joint probability densities are shown in logarithmic scale for better visibility. Contours are in the range log(JPDF) $\in [-2; 2]$ with a step size of 0.25. The location of the mode is highlighted by the white cross symbol ×. To the side of each JPDF is the marginal pdf of $\kappa^+\delta_L^0$ (top) and G^+ (right) respectively. Quadrant probabilities are written in gray color.

as a reliable marker of thermodiffusive instability. These correlations offer a quantitative and physically-interpretable complement to integral measurements of the stretch factor which lacks explicit information on local burning. They also provide an experimentally-accessible metric to gauge the strength of the instability in hydrogen-containing flames, in absence of local fuel consumption rate data which is hardly accessible experimentally. The gradual transition from a thermo-diffusively stable (stoichiometric methane-air) to an unstable (lean hydrogen-air flame) and implications on local burning are also examined for the first time in this context, as past experiments and direct numerical simulations have focused on either pure methane or pure hydrogen-air flames.

CRediT authorship contribution statement

Oussama Chaib: Conceptualization, Data analysis, Visualization, Writing. **Simone Hochgreb:** Conceptualization, Supervision, Reviewing and editing. **Isaac Boxx:** Design of experiments, Data acquisition, Reviewing and editing.

Declaration of competing interest

The authors declare that they have no known competing financial interests or personal relationships that could have appeared to influence the work reported in this paper.

Acknowledgments

Oussama Chaib is supported by an EPSRC DTP Studentship (EP/T5 17847/1, reference no. 2598182, University of Cambridge). Experimental work was supported by European Research Council (ERC) grant no. 682,383 (HyBurn) under the European Union's Horizon 2020 research and innovation programme. For the purpose of open access, the authors have applied a Creative Commons Attribution (CC BY) licence to any Author Accepted Manuscript version arising.

References

[1] S.R. Bell, M. Gupta, Extension of the lean operating limit for natural gas fueling of a spark ignited engine using hydrogen blending, Combust. Sci. Technol. 123 (1–6) (1997) 23–48.

[2] R.W. Schefer, Hydrogen enrichment for improved lean flame stability, Int. J. Hydrogen Energy (2003) 11.

[3] F. Halter, C. Chauveau, I. Gokalp, Characterization of the effects of hydrogen addition in premixed methane/air flames, Int. J. Hydrogen Energy 32 (13) (2007) 2585–2592.

[4] N. Bouvet, F. Halter, C. Chauveau, Y. Yoon, On the effective Lewis number formulations for lean hydrogen/hydrocarbon/air mixtures, Int. J. Hydrogen Energy 38 (14) (2013) 5949–5960.

[5] J.B. Bell, R.K. Cheng, M.S. Day, I.G. Shepherd, Numerical simulation of Lewis number effects on lean premixed turbulent flames, Proc. Combust. Inst. 31 (1) (2007) 1309–1317.

[6] L. Berger, K. Kleinheinz, A. Attili, H. Pitsch, Characteristic patterns of thermodiffusively unstable premixed lean hydrogen flames, Proc. Combust. Inst. 37 (2) (2019) 1879–1886.

[7] M. Haq, C. Sheppard, R. Woolley, D. Greenhalgh, R. Lockett, Wrinkling and curvature of laminar and turbulent premixed flames, Combust. Flame 131 (1–2) (2002) 1–15.

[8] Y.-C. Chen, R.W. Bilger, Experimental investigation of three-dimensional flame-front structure in premixed turbulent combustion, Combust. Flame 138 (1–2) (2004) 155–174.

[9] S. Hochgreb, How fast can we burn, 2.0, Proc. Combust. Inst. 39 (2) (2023) 2077–2105.

[10] L. Berger, A. Attili, H. Pitsch, Synergistic interactions of thermodiffusive instabilities and turbulence in lean hydrogen flames, Combust. Flame 244 (2022) 112254.

[11] M. Baum, T.J. Poinsot, D.C. Haworth, N. Darabiha, Direct numerical simulation of $H_2/O_2/N_2$ flames with complex chemistry in two-dimensional turbulent flows, J. Fluid Mech. 281 (1994) 1–32.

[12] M. Day, J. Bell, P.-T. Bremer, V. Pascucci, V. Beckner, M. Lijewski, Turbulence effects on cellular burning structures in lean premixed hydrogen flames, Combust. Flame 156 (5) (2009) 1035–1045.

[13] M. Day, S. Tachibana, J. Bell, M. Lijewski, V. Beckner, R.K. Cheng, A combined computational and experimental characterization of lean premixed turbulent low Swirl Laboratory flames II. Hydrogen flames, Combust. Flame 162 (5) (2015) 2148–2165.

[14] T. Howarth, A. Aspden, An empirical characteristic scaling model for freely-propagating lean premixed hydrogen flames, Combust. Flame 237 (2022) 111805.

[15] L. Berger, M. Grinberg, B. Jürgens, P.E. Lapenna, F. Creta, A. Attili, H. Pitsch, Flame fingers and interactions of hydrodynamic and thermodiffusive instabilities in laminar lean hydrogen flames, Proc. Combust. Inst. 39 (2) (2023) 1525–1534.

[16] M.S. Day, J.B. Bell, R.K. Cheng, S. Tachibana, V.E. Beckner, M.J. Lijewski, Cellular burning in lean premixed turbulent hydrogen-air flames: Coupling experimental and computational analysis at the laboratory scale, J. Phys.: Conf. Ser. 180 (1) (2009) 012031.

[17] J. Pareja, T. Lipkowicz, E. Inanc, C.D. Carter, A. Kempf, I. Boxx, An experimental/numerical investigation of non-reacting turbulent flow in a piloted premixed Bunsen burner, Exp. Fluids 63 (1) (2022) 33.

[18] C.K. Law, C.J. Sung, Structure, aerodynamics, and geometry of premixed flamelets, Prog. Energy Combust. Sci. (2000) 47.

[19] D.G. Goodwin, H.K. Moffat, I. Schoegl, R.L. Speth, B.W. Weber, Cantera: An object-oriented software toolkit for chemical kinetics, thermodynamics, and transport processes, 2022, Version 2.6.0.

[20] G.P. Smith, D.M. Golden, M. Frenklach, N.W. Moriarty, B. Eiteneer, M. Goldenberg, C.T. Bowman, R.K. Hanson, S. Song, W.C. Gardiner, Jr., V.V. Lissianski, Z. Qin, GRI-Mech 3.0, 1999.

[21] O. Chaib, Y. Zheng, S. Hochgreb, I. Boxx, Hybrid algorithm for the detection of turbulent flame fronts, Exp. Fluids 64 (5) (2023) 104.

[22] A. Kushwaha, P. Kasthuri, S.A. Pawar, R.I. Sujith, I. Chterev, I. Boxx, Dynamical characterization of thermoacoustic oscillations in a hydrogen-enriched partially premixed swirl-stabilized methane/air combustor, J. Eng. Gas Turbines Power 143 (12) (2021) 121022.
[23] T.M. Wabel, A.W. Skiba, J.F. Driscoll, Turbulent burning velocity measurements: Extended to extreme levels of turbulence, Proc. Combust. Inst. 36 (2) (2017) 1801–1808.
[24] R.S.M. Chrystie, I.S. Burns, J. Hult, C.F. Kaminski, On the improvement of two-dimensional curvature computation and its application to turbulent premixed flame correlations, Meas. Sci. Technol. 19 (12) (2008) 125503.
[25] J. Driscoll, Turbulent premixed combustion: Flamelet structure and its effect on turbulent burning velocities, Prog. Energy Combust. Sci. 34 (1) (2008) 91–134.